Published in final edited form as:

Magn Reson Med. 1995 December ; 34(6): 910–914.

The Rician Distribution of Noisy MRI Data

Hákon Gudbjartsson and **Samuel Patz**

From the Massachusetts Institute of Technology Department of EECS (H.G.), and Harvard Medical School, and Brigham and Women's Hospital (S.P.), Department of Radiology, Boston, Massachusetts

Abstract

The image intensity in magnetic resonance magnitude images in the presence of noise is shown to be governed by a Rician distribution. Low signal intensities (SNR < 2) are therefore biased due to the noise. It is shown how the underlying noise can be estimated from the images and a simple correction scheme is provided to reduce the bias. The noise characteristics in phase images are also studied and shown to be very different from those of the magnitude images. Common to both, however, is that the noise distributions are nearly Gaussian for SNR larger than two.

Keywords

Rician; Rayleigh; Gaussian; noise

INTRODUCTION

It is common practice to assume the noise in magnitude MRI images is described by a Gaussian distribution. The power of the noise is then often estimated from the standard deviation of the pixel signal intensity in an image region with no NMR signal. This can, however, lead to an approximately 60% underestimation of the true noise power. Here we will show that there is a simple analytical relationship between the true noise power and the estimated noise variance.

The characteristics of noise in magnitude MRI images has been studied before by Henkelman and the reader is referred to ref. 1 for the formulation of the problem. Henkelman analyzed the problem numerically and did not provide analytical expressions for the noise characteristics. The noise characteristics of quadrature detection, however, have been thoroughly analyzed and documented in applications to communication (2–3).

During the preparation of this manuscript, we have come across several references in the MRI literature that describe some of the results presented here. Edelstein *et al.* (4) showed that pure noise in magnitude images is governed by the Rayleigh distribution and later Bernstein *et al.* (5) provided the closed form solution of the more general Rician distribution in their study on detectability in MRI. Brummer *et al.* (6) have also exploited the Rayleigh

Address correspondence to: Hákon Gudbjartsson, Department of Radiology/BWH, 221 Longwood Avenue, Boston, MA 02115.

distribution in a histogram analysis for automatic evaluation of the “true noise” in application to image segmentation.

In this paper we will review the theoretical distributions for the noise in magnitude images and then we supplement it with the exact expression for the noise distribution in phase images as well. A very simple postprocessing scheme is proposed to correct for the bias due to the Rician distribution of the noisy magnitude data. The statistical properties of the correction scheme are studied and compared with a similar correction scheme for power images, proposed earlier independently by Miller and Joseph (7) and McGibney and Smith (8).

THEORY

Magnitude images are most common in MRI because they avoid the problem of phase artifacts by deliberately discarding the phase information. The signal is measured through a quadrature detector that gives the real and the imaginary signals. We will assume the noise in each signal to have a Gaussian distribution with zero mean and each channel will be assumed to be contaminated with white noise.

The real and the imaginary images are reconstructed from the acquired data by the complex Fourier transform. Because the Fourier transform is a linear and orthogonal transform, it will preserve the Gaussian characteristics of the noise. Furthermore, the variance of the noise will be uniform over the whole field of view and, due to the Fourier transform, the noise in the corresponding real and imaginary voxels can be assumed uncorrelated.

There are many factors that influence the final signal-to-noise ratio (SNR) in the real and imaginary images. Not only is the noise associated with the receiving coil resistance, but also with inductive losses in the sample (9). Which one is the dominant source will depend on the static magnetic field (B_0) and the sample volume size. Furthermore, the final image noise will depend on the image voxel size, the receiver bandwidth and the number of averages in the image acquisition (10).

Magnitude Images

The magnitude images are formed by calculating the magnitude, pixel by pixel, from the real and the imaginary images. This is a nonlinear mapping and therefore the noise distribution is no longer Gaussian.

The image pixel intensity in the absence of noise is denoted by A and the measured pixel intensity by M. In the presence of noise, the probability distribution for M can be shown to be given by (2, 3)

$$p_M(M)=\frac{M}{\sigma^2}e^{-(M^2+A^2)/2\sigma^2}I_0\left(\frac{A\cdot M}{\sigma^2}\right) \quad [1]$$

where I_0 is the modified zeroth order Bessel function of the first kind and σ denotes the standard deviation of the Gaussian noise in the real and the imaginary images (which we assume to be equal). This is known as the *Rice* density and is plotted in Fig. 1 for different values of the SNR, A/σ. As can be seen the Rician distribution is far from being Gaussian for small SNR ($A/\sigma \leq 1$). For ratios as small as $A/\sigma = 3$, however, it starts to approximate the Gaussian distribution.

Note that the mean of the distributions, $\bar{M}/\sigma$, which is shown by the vertical lines in Fig. 1, is not the same as A/σ. This bias is due to the nonlinear transform of the noisy data.

A special case of the Rician distribution is obtained in image regions where only noise is present, $A = 0$. This is better known as the *Rayleigh* distribution and Eq. [1] reduces to

$$p_M(M) = \frac{M}{\sigma^2} e^{-M^2/2\sigma^2} \quad [2]$$

This Rayleigh distribution governs the noise in image regions with no NMR signal. The mean and the variance for this distribution can be evaluated analytically and are given by (11)

$$\overline{M} = \sigma\sqrt{\pi/2} \text{ and } \sigma_M^2 = (2 - \pi/2)\sigma^2 \quad [3]$$

These relations can be used to estimate the "true" noise power, σ^2, from the magnitude image. Another interesting limit of Eq. [1] is when the SNR is large.

$$p_M(M) \approx \frac{1}{\sqrt{2\pi\sigma^2}} e^{-1(M-\sqrt{A^2+\sigma^2})^2/2\sigma^2} \quad [4]$$

This equation shows that for image regions with large signal intensities the noise distribution can be considered as a Gaussian distribution with variance σ^2 and mean $\sqrt{A^2+\sigma^2}$. This trend is clearly seen for large ratios, A/σ, in Fig. 1.

Phase Images

Phase images, which are commonly used in flow imaging, are reconstructed from the real and the imaginary images by calculating pixel by pixel the arctangent of their ratio. This is a nonlinear function and therefore we no longer expect the noise distribution to be Gaussian. Indeed, the distribution of the phase noise, $\Delta\theta = \theta - \bar{\theta}$, is given by ref 3

$$p_{\Delta\theta}(\Delta\theta)=\frac{1}{2\pi}e^{-A^2/2\sigma^2}\left[1+\frac{A}{\sigma}\sqrt{2\pi}\cos\Delta\theta\; e^{A^2\cos^2\Delta\theta/2\sigma^2}\cdot\frac{1}{\sqrt{2\pi}}\int_{-\infty}^{\frac{A\cos\Delta\theta}{\sigma}}e^{-x^2/2}dx\right] \quad [5]$$

Although the general expression for the distribution of $\Delta\theta$ is complicated, the two limits of A, $A = 0$ and $A \gg \sigma$, turn out to yield simple distributions.

In image regions where there is only noise, $A = 0$, Eq. [5] reduces to

$$p_{\Delta\theta}(\Delta\theta)=\begin{cases}\frac{1}{2\pi}\text{if } -\pi<\Delta\theta<\pi\\ 0 \text{ otherwise}\end{cases} \quad [6]$$

This result is obvious since the complex data, which only consists of the noise, “points in all directions” with the same probability.

For large SNR, $A \gg \sigma$, it is easy to see that the deviation in the phase angle, $\Delta\theta$, due to the noise will be small. The integral in Eq. [5] will therefore be close to 1 and the second term in the brackets will therefore dominate the constant 1. Equation [5] therefore reduces to

$$\begin{aligned}p_{\Delta\theta}(\Delta\theta) &\approx \frac{A\cos\Delta\theta}{\sigma\sqrt{2\pi}}\exp\left[\frac{-A^2(1-\cos^2\Delta\theta)}{2\sigma^2}\right]\\ &\approx \frac{1}{\sqrt{2\pi(\sigma/A)^2}}\exp\left[\frac{-\Delta\theta^2}{2(\sigma/A)^2}\right]\end{aligned} \quad [7]$$

The noise distribution in the phase angle can therefore be considered as a zero mean Gaussian distribution, when $A \gg \sigma$. This result is not surprising because when the pixel intensity is large, all deviations parallel to the complex pixel intensity can be ignored. Also the phase variations, due to the noise which is orthogonal to the complex pixel intensity, can be linearized as σ/A, where σ represents the orthogonal part of the noise.

The standard deviations for the phase noise can in general be calculated by using Eq. [5], however, for the two special cases in Eqs. [6] and [7] it is given by

$$\sigma_{\Delta\theta}=\begin{cases}\frac{\sigma}{A}\text{if } A\gg\sigma\\ \sqrt{\frac{2\pi^2}{3}}\text{ if } A=0\end{cases} \quad [8]$$

Figure 2 shows the distribution in the phase noise, evaluated by Eq. [5], for several signal to noise ratios. The Gaussian approximation is also shown by the dotted line for $A/\sigma = 3$. Clearly the Gaussian approximation is very good even for fairly small signal to noise ratios.

Phase images are sometimes weighted by the magnitude data, to reduce phase variations in regions with no signal. The general noise distribution for such images is nontrivial. For regions with large SNR one can show that the distribution approaches a Gaussian distribution whose standard deviation is σ.

BIAS REDUCTION IN MAGNITUDE DATA

For large SNR Eq. [4] shows that the mean of M is not the true image intensity A, but approximately $\sqrt{A^2+\sigma^2}$. This is a small deviation for large SNR, however, when the SNR is small this bias has to be considered. We will continue to approximate the mean by the simple expression $\sqrt{A^2+\sigma^2}$ for all SNR, but for an exact analytical evaluation of the mean of Eq. [1] see refs. 2 and 5. Figure 1 shows the mean of the Rician distribution for several values of A/σ plotted as a straight vertical line. Henkelman suggested a look-up table correction scheme to correct for this bias (1). We, however, suggest a much simpler correction scheme.

To reduce the bias the following postprocessing correction scheme is suggested:

$$\tilde{A}=\sqrt{|M^2-\sigma^2|} \quad [9]$$

The probability distribution for the corrected signal, $\tilde{A}$, is then given by

$$p_{\tilde{A}}(\tilde{A})=\begin{cases}\frac{\tilde{A}\cdot p_M(\sqrt{\sigma^2+\tilde{A}^2})}{\sqrt{\sigma^2+\tilde{A}^2}}+\frac{\tilde{A}\cdot p_M(\sqrt{\sigma^2-\tilde{A}^2})}{\sqrt{\sigma^2-\tilde{A}^2}} & \text{if } \tilde{A}<\sigma \\ \frac{\tilde{A}\cdot p_M(\sqrt{\sigma^2+\tilde{A}^2})}{\sqrt{\sigma^2+\tilde{A}^2}} & \text{if } \tilde{A}\geq\sigma\end{cases} \quad [10]$$

where p_M is defined by Eq. [1]. The distribution of $\tilde{A}$ is shown in Fig. 3 for several signal to noise ratios. We see that the bias is greatly reduced, however, the corrected distribution is not Gaussian. For ratios of $A/\sigma > 2$ the corrected distribution is however very close to being a Gaussian. Table 1 lists the mean and the standard deviation of the corrected and uncorrected distributions.

A different, but somewhat similar, correction scheme has been proposed for power images, independently by Miller and Joseph (7) and McGibney and Smith (8), to perform quantitative analysis on low SNR images and as an unbiased SNR estimate, respectively. It is interesting to compare this with our correction scheme, described above.

Their correction scheme is based on the simple relationship between the mean of the measured power and the true image power, namely $M^2 = A^2 + 2\sigma^2$ (1, 7). Their correction scheme is therefore simply

$$\tilde{A}^2 = M^2 - 2\sigma^2 \quad [11]$$

We have found that the resulting distribution for the corrected power, $\tilde{A}^2$, is given by

$$p_{\tilde{A}^2}(\tilde{A}^2) = \frac{1}{2\sigma^2} e^{-(\tilde{A}^2 + 2\sigma^2 + A^2)/2\sigma^2} I_0\left(\frac{A \cdot \sqrt{\tilde{A}^2 + 2\sigma^2}}{\sigma^2}\right) \quad [12]$$

The mean of $\tilde{A}^2$ gives an unbiased estimate of A^2. We have calculated the variance of $\tilde{A}^2$ and found it to be given by

$$\sigma^2_{\tilde{A}^2} = 4A^2\sigma^2 + 4\sigma^4 \quad [13]$$

Figure 4 shows the distribution of M^2 and $\tilde{A}^2$ as the original and the corrected image power, respectively. The distributions are clearly far from being Gaussian at low SNR although their mean is always the true mean, A^2. This can lead to some ambiguities, when information is extracted from corrected power data, because least-squares fitting techniques, such as nonlinear chi-square minimization, assume Gaussian deviation that is fully characterized by its standard deviation. For large SNR, however, one can show that the distribution for $\tilde{A}^2$ becomes approximately a Gaussian distribution of $\sqrt{\tilde{A}^2}$ with a mean A^2 and variance given by Eq. [13]. The variance dependence on the power strength is an issue which has to be taken into account, for accurate fitting. Unlike ours, their correction scheme, originally proposed to fit mono-exponentials (7), cannot be used when the signal has a multi-exponential nature. Finally, analysis based on statistics from a region of interest will be sensitive to any variations in A, because the mean of the distribution is a function of A^2.

MODEL VERIFICATION

A magnitude image was collected and reconstructed on a 1.5T GE Signa imager (General Electric Medical Systems, Milwaukee, WI). A large region, which contained only noise and was without any phase artifacts such as motion artifacts, was selected. Figure 5 shows a histogram of the image intensity plotted versus the theoretical Rayleigh probability distribution ($A = 0$). Note that the image intensity has been rounded by the imager to integer numbers. The true noise variance, σ, was estimated from the mean of the region, by using Eq. [3]. The mean was found from the histogram by assuming that the data had been rounded to its nearest integer.

The quality of the fit of the data, shown in Fig. 5, to the Rayleigh distribution was determined as follows. The histogram was divided into 10 bins such that for each bin the theoretical bin distribution could be accurately approximated by a Gaussian distribution. A

chi-square test (11) using 8 degrees of freedom (one degree is lost due to a finite number of counts and one due to the estimation of σ from the data) showed that $\chi^2 = 29$. Although the fit in Fig. 5 may look good, this is too large a number to statistically verify the hypothesis of Rayleigh distributed noise. This disagreement is interesting considering the fact that Henkelman (1) calculated the ratio of the average value to the standard deviation of the signal over a series of 10 images and found it to be given by 1.91 ± 0.01, in excellent agreement with Eq. [3]. The chi-square test is, however, more sensitive to the fine details in the noise distribution than the ratio test. As a second test we also calculated the ratio $\bar{M}/\sigma_M$ over a series of ten images and found it to equal 2.06 ± 0.01. This disagreement with Eq. [3] indicates that the noise characteristics of our imaging system do not fully comply with the simplistic noise model presented in this document. One possible source of error might be some correlations in the noise. The next step was therefore to calculate the auto-correlation of the noise, and the results are shown in Fig. 6. According to our model, Eqs. [2] and [3], the ratio of the correlation coefficient $C(i, j)$ to C(0, 0), is given by

$$\frac{C(i,j)}{C(0,0)} = \frac{\overline{M_1 M_2}}{\overline{M^2}} = \frac{\overline{M^2}}{\sigma_M^2 + \overline{M^2}} = \frac{\pi}{4}, (i,j) \neq (0,0) \quad [14]$$

Apart from the extra correlation in the vicinity of (0, 0), resulting from the point spread function of the Fermi low-pass filter, the agreement with Eq. [14] is only with accuracy of ca. 3%.

CONCLUSION

In this note we have given the theoretical noise distributions for magnitude and phase images and shown how these distributions reduce to the Gaussian distribution for even fairly small SNR. We also introduced a simple postprocessing scheme to correct for the noise dependent bias in magnitude images where the SNR is poor. The statistical properties of our correction scheme were compared with an existing correction scheme for power images.

We were not able to verify the mathematical model for the Rayleigh distribution statistically, however, the analytical distributions provided here are in good agreement with earlier results (1). Some unknown manipulations of the data by the reconstruction program seems to invalidate the simplistic assumptions made in the formulation of the problem. As shown in Fig. 6 the disagreement is however very small.

References

1. Henkelman RM. Measurement of signal intensities in the presence of noise in MR images. Med Phys. 1985; 12:232–233. Erratum in 13, 544 (1986). [PubMed: 4000083]
2. Rice SO. Mathematical analysis of random noise. Bell System Tech J. 1944; 23:282. Reprinted by N. Wax, Selected Papers on Noise and Stochastic Process, Dover Publication, 1954, QA273W3.
3. Lathi, BP. Modern Digital and Analog Communication Systems. Hault-Saunders International Edition; Japan: 1983.
4. Edelstein WA, Bottomley PA, Pfeifer LM. A signal-to-noise calibration procedure for NMR imaging systems. Med Phys. 1984; 11(2):180–185. [PubMed: 6727793]

5. Bernstein MA, Thomasson DM, Perman WH. Improved detectability in low signal-to-noise ratio magnetic resonance images by means of a phase-corrected real reconstruction. Med Phys. 1989; 15(5):813–817.
6. Bmmmer ME, Mersereau RM, Eisner RL, Lewine RRJ. Automatic detection of brain contours in MRI data sets. IEEE Trans Med Imaging. 1993; 12(2):153–166. [PubMed: 18218403]
7. Miller AJ, Joseph PM. The use of power images to perform quantitative analysis on low SNR MR images. Magn Reson Imaging. 1993; 11:1051–1056. [PubMed: 8231670]
8. McGibney G, Smith MR. An unbiased signal-to-noise ratio measure for magnetic resonance images. Med Phys. 1993; 20(4):1077–1078. [PubMed: 8413015]
9. Hoult DI, Lauterbur PC. The sensitivity of the zeugmatographic experiment involving human samples. J Magn Reson. 1979; 34:425–433.
10. Edelstein WA, Glover GH, Hardy CJ, Redington W. The intrinsic signal-to-noise ratio in NMR imaging. Magn Reson Med. 1986; 3:604–618. [PubMed: 3747821]
11. Papoulis, A. Probability, Random Variables, and Stochastic Processes. 3. McGraw-Hill Inc.; New York: 1991.

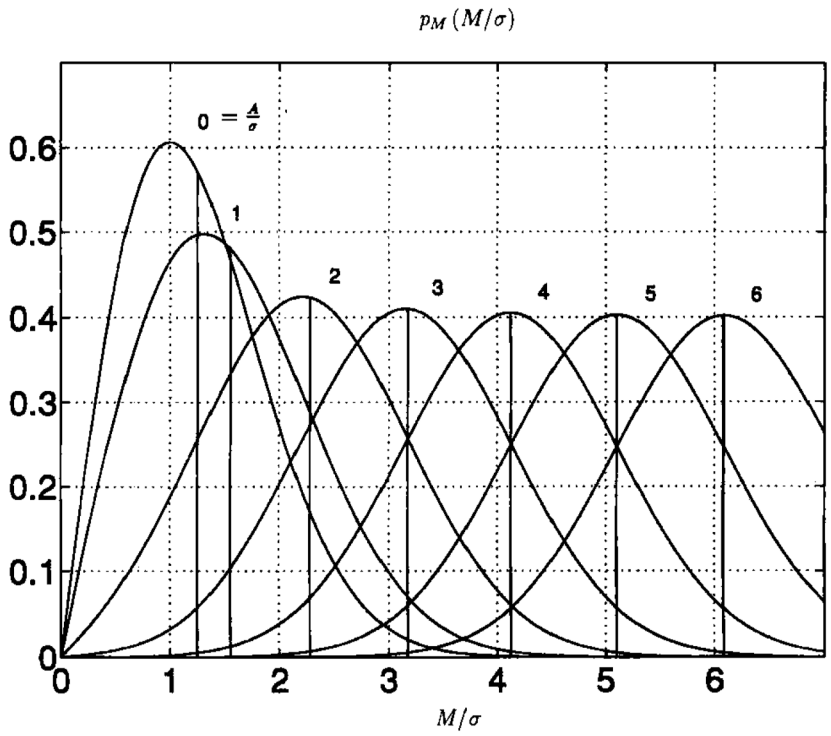

FIG. 1.

The Rician distribution of M for several signal to noise ratios, A/σ, and the corresponding means.

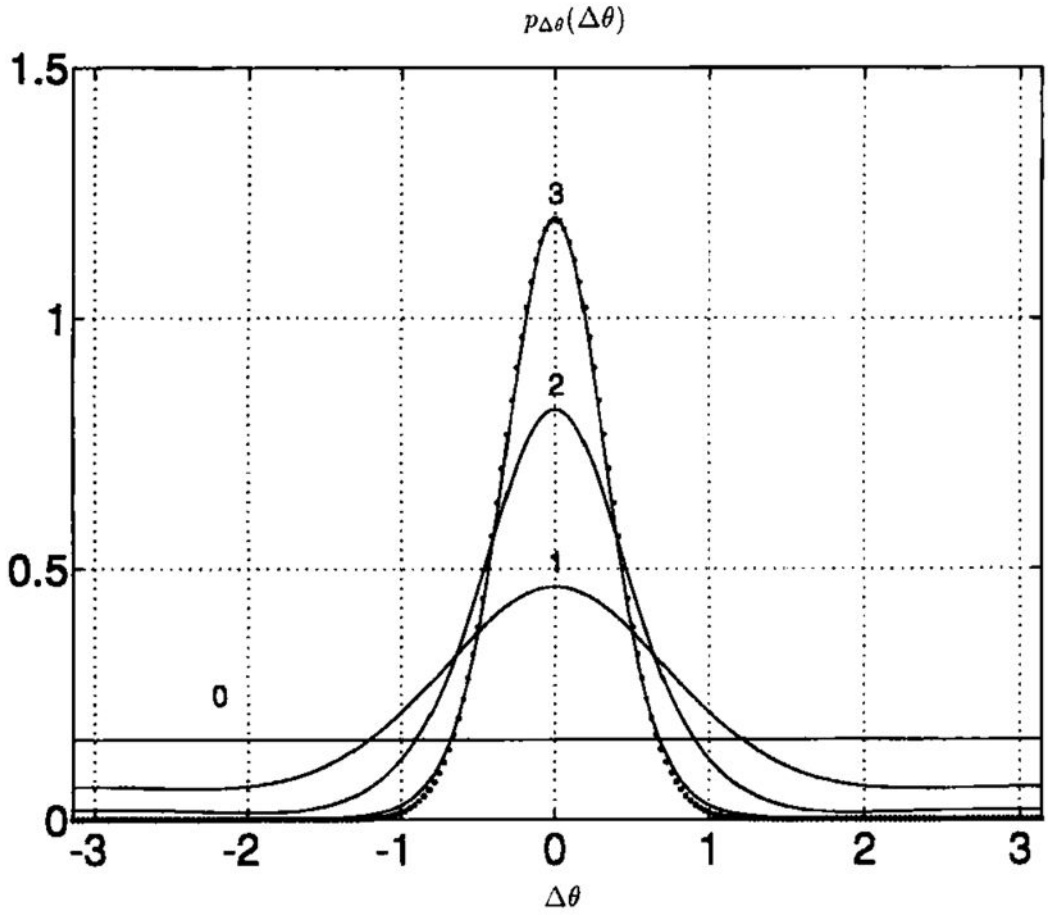

FIG. 2.

The distribution of the phase noise for several signal to noise ratios, A/σ. The Gaussian approximation is shown with a dotted line for $A/\sigma = 3$.

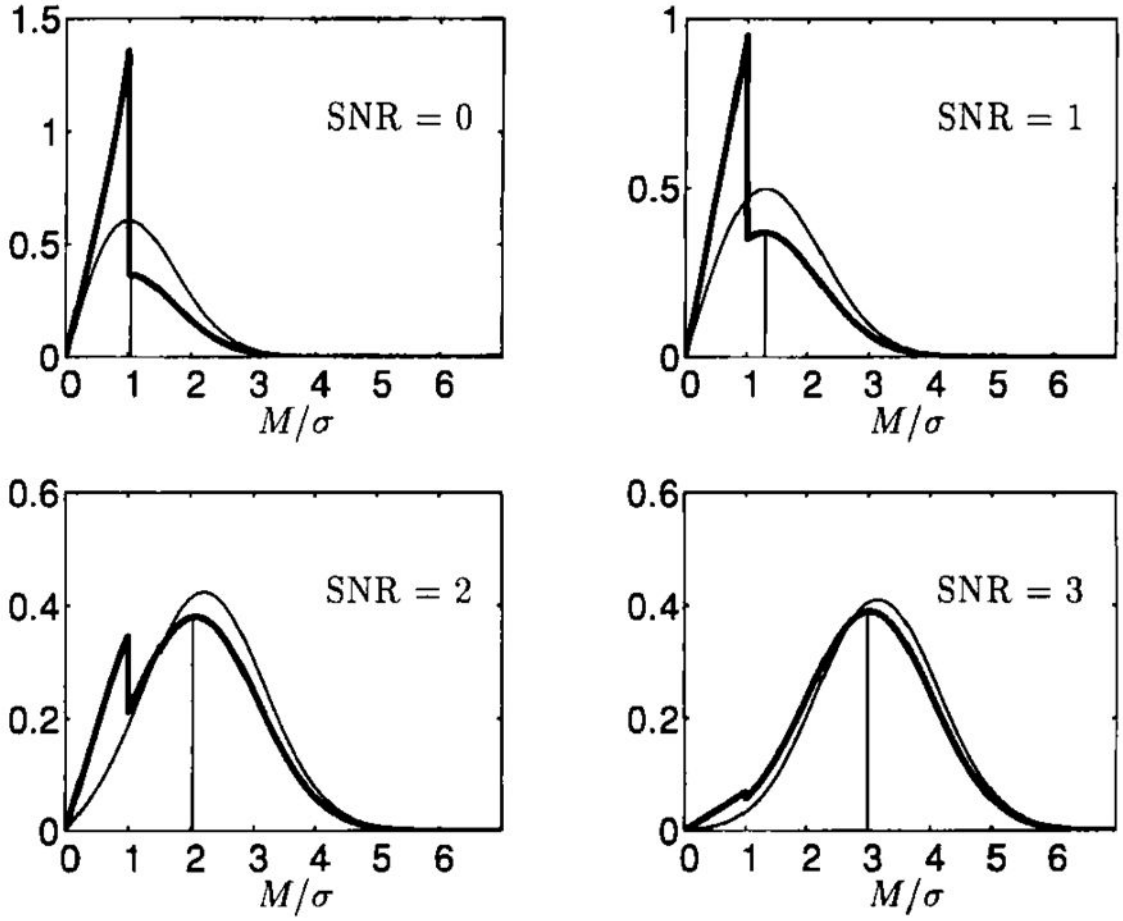

FIG. 3.

The distribution of the corrected pixel intensity, $\tilde{A}$ (bold), compared with the Rician distribution of M for several signal to noise ratios. The mean of the corrected distribution, A, is shown with a vertical line.

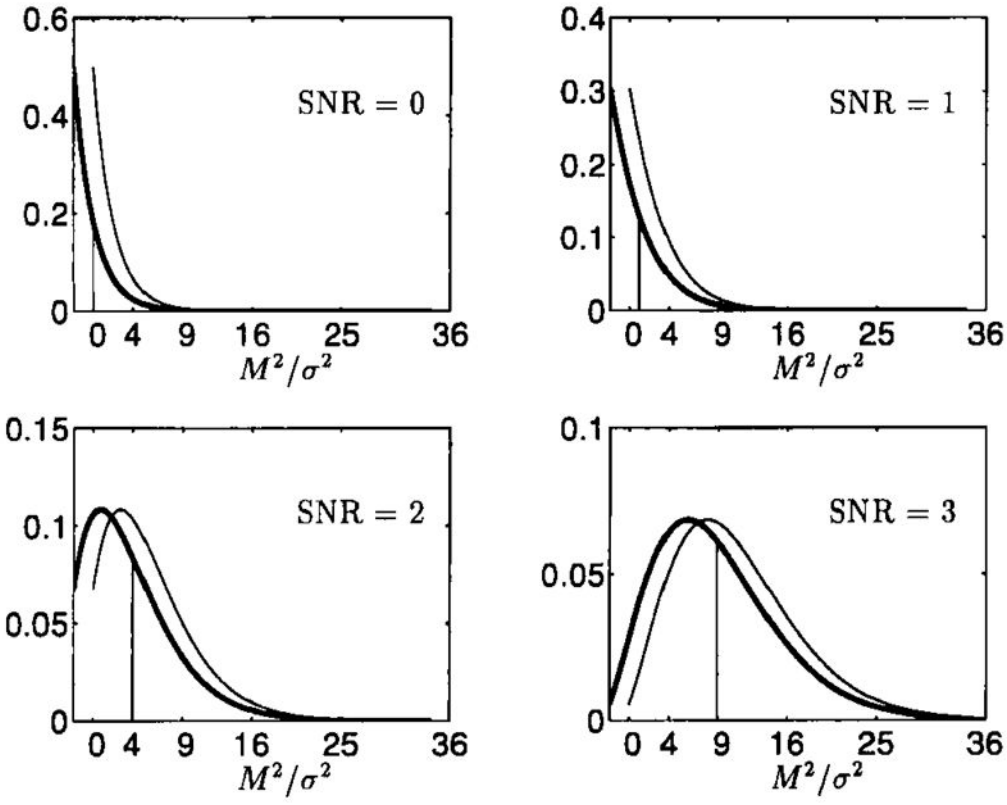

FIG. 4.

The distribution of the corrected pixel power (7), $\tilde{A}^2$ (bold), compared with the distribution of the measured power, M^2, for several signal to noise ratios. The mean of the corrected distribution, $\overline{\tilde{A}^2} = A^2$, is shown with a vertical line.

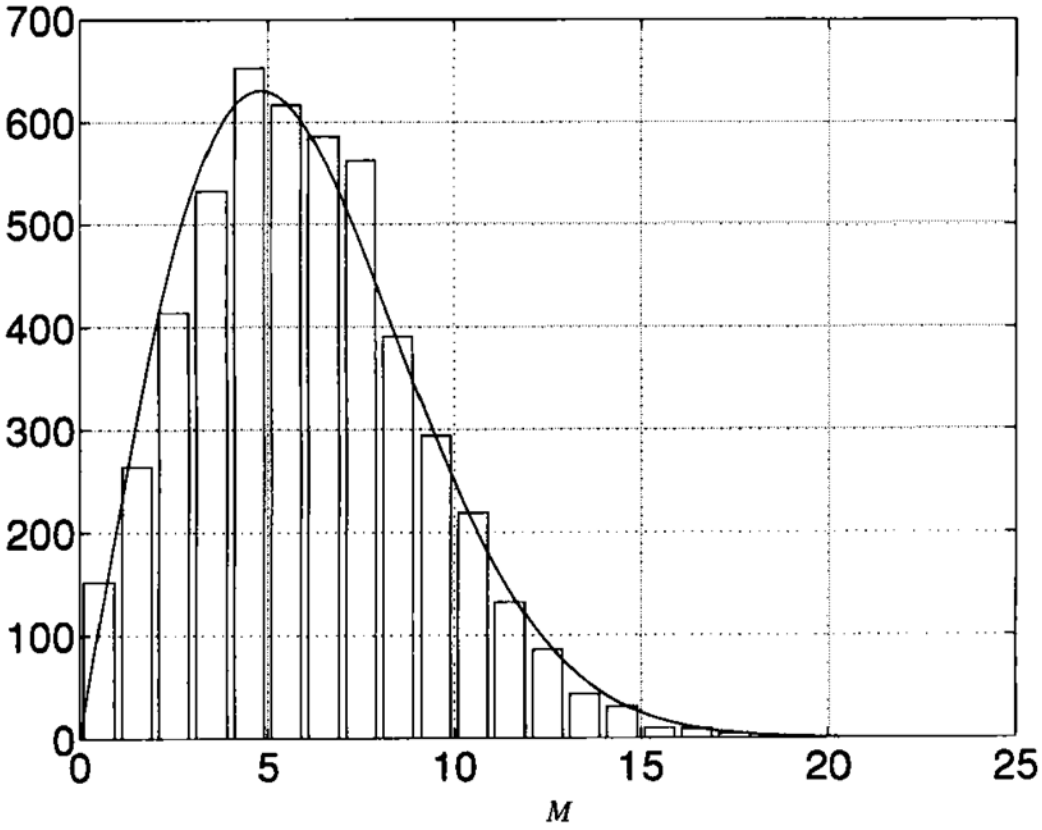

FIG. 5.

Histogram of the pixel intensity from a region with $N = 5000$ pixels. The solid line is the corresponding Rayleigh distribution, estimated from the mean of the histogram.

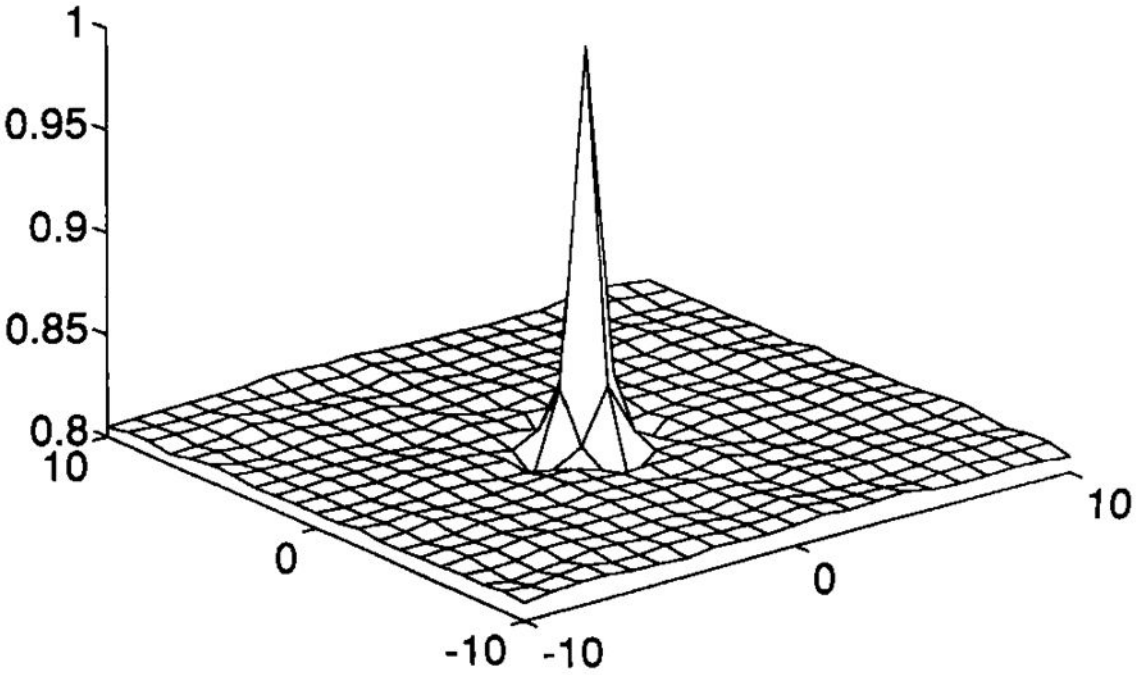

FIG. 6.

The normalized autocorrelation function of the image noise shows some extra correlation due to the Fermi lowpass filtering of the data. Otherwise the agreement with Eq. [14] is good.

Table 1

Some Statistical Properties of the Rician Distribution and the Correction Scheme for Several Signal-to-Noise Ratios

A/σ	$\bar{A}/\sigma$	$\sigma_{\bar{A}}/\sigma$	$\bar{M}/\sigma$	σ_M/σ
0	1.03	0.35	1.25	0.43
0.5	1.10	0.42	1.33	0.48
1	1.30	0.59	1.55	0.60
1.5	1.61	0.79	1.87	0.73
2	2.03	0.96	2.27	0.84
2.5	2.50	1.04	2.71	0.90
3	3.00	1.07	3.17	0.93